

Supporting Information

Exploring the Impact of Atomic Lattice Deformation on Oxygen Evolution Reaction based on a Sub 5 nm Pure Face-centred Cubic High-entropy Alloy Electrocatalyst

Kang Huang, Bowei Zhang, Junsheng Wu*, Tianyuan Zhang, Dongdong Peng, Xun Cao, Zhan Zhang, Zhong Li, and Yizhong Huang*

Dr. K. Huang, Pro. B. Zhang, Pro. J. Wu, Dr. Z. Zhang

Institute of Advanced Materials and Technology, University of Science and Technology Beijing, Beijing, 100083, China

E-mail: wujs76@163.com

Dr. D. Peng, Dr. X. Cao, Pro. Y. Huang

School of Materials Science and Engineering, Nanyang Technological University, 50 Nanyang Avenue, 639798, Singapore

E-mail: yzhuang@ntu.edu.sg

Dr. T. Zhang

Department of Chemistry, University of Washington, Seattle, WA, 98195, United States

Dr. Z. Li

Department of Chemical and Biomolecular Engineering, Ohio University, Athens; OH; 45701, United States

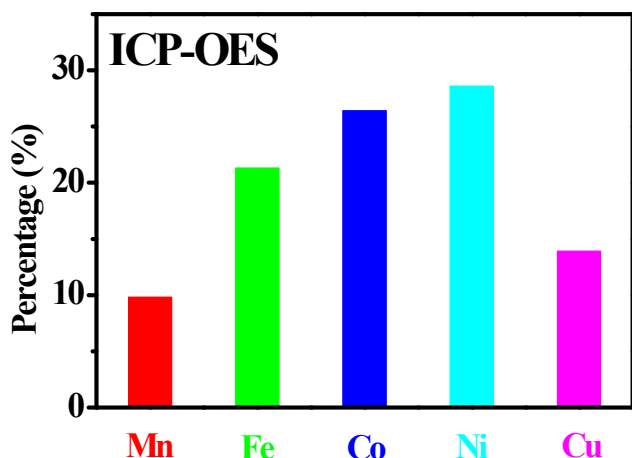


Figure S1. ICP-OES of HEA nanoparticles. Corresponding element content of HEAN@NPC/CC-450 catalyst.

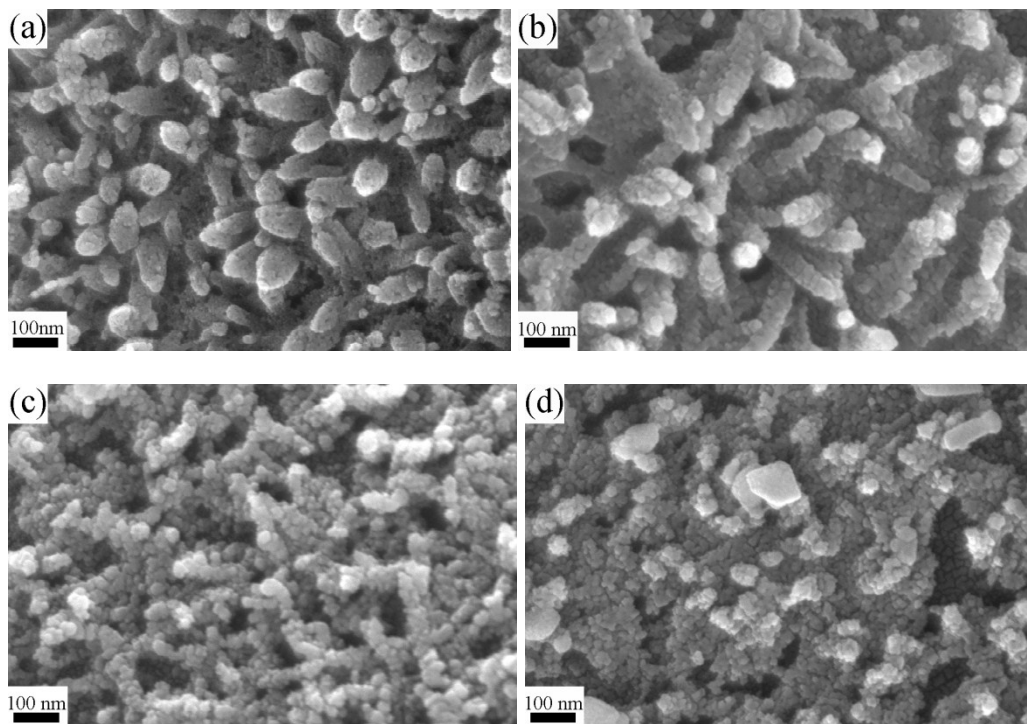


Figure S2. Morphological characterization. (a-d) FESEM images of HEAN@NPC/CC-350, HEAN@NPC/CC-400, HEAN@NPC/CC-500, and HEAN@NPC/CC-600, respectively.

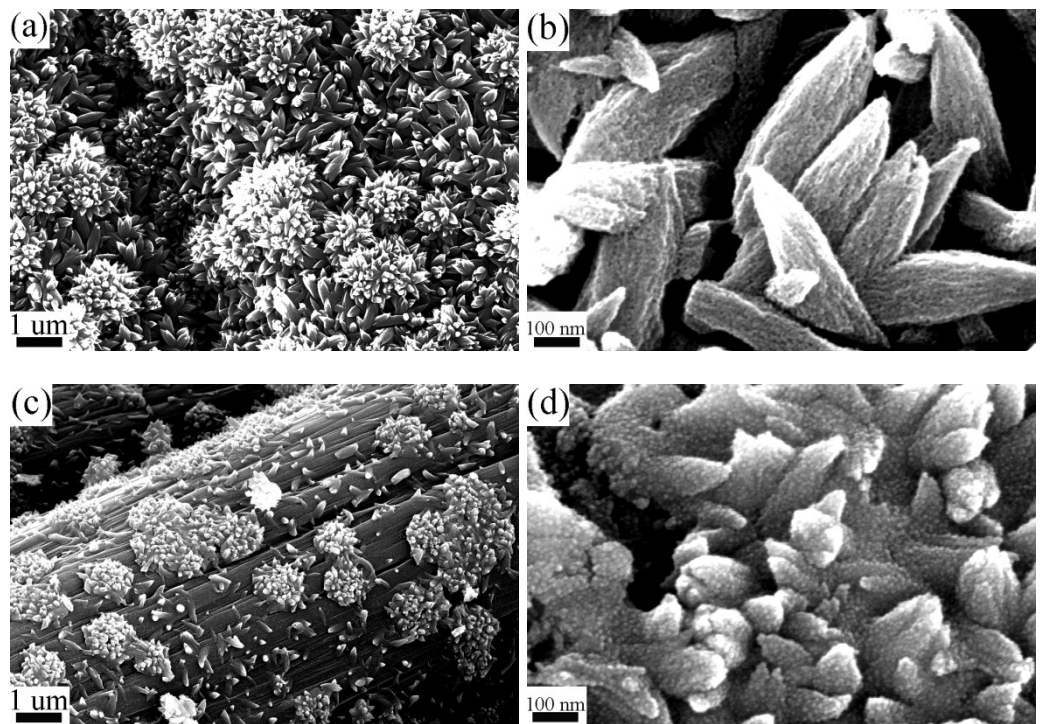


Figure S3. Morphological characterization. (a-b) FESEM images of FeCoNi MOFs/CC, (c-d) FESEM images of FeCoNi/CC.

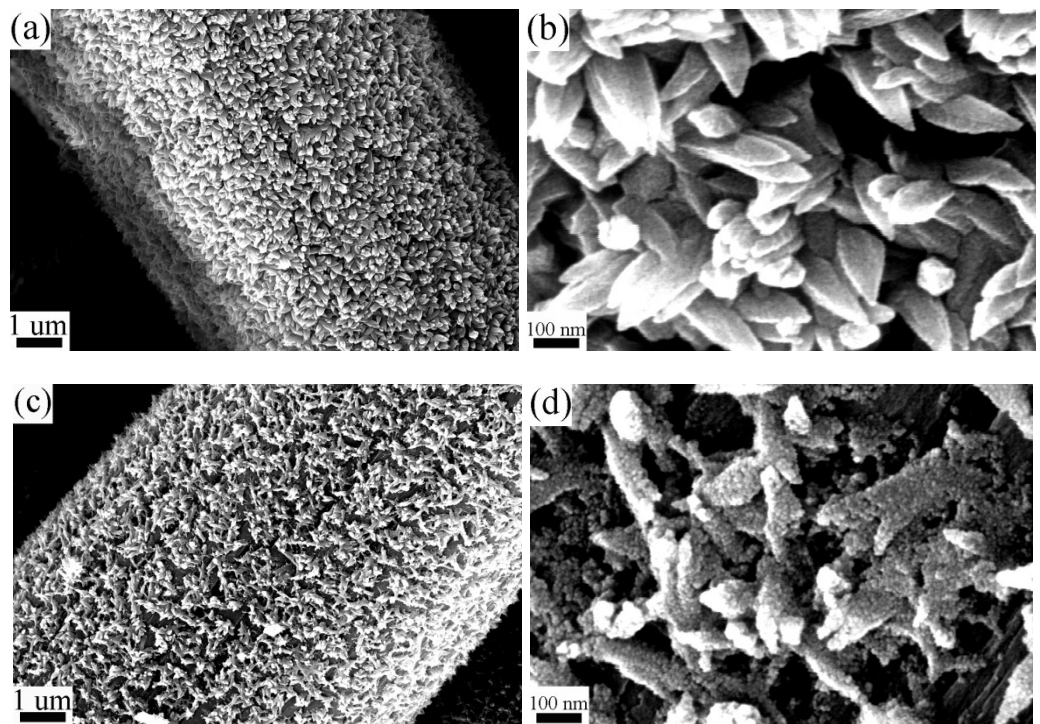


Figure S4. Morphological characterization. (a-b) FESEM images of MnFeCoNi MOFs/CC, (c-d) FESEM images of MnFeCoNi/CC.

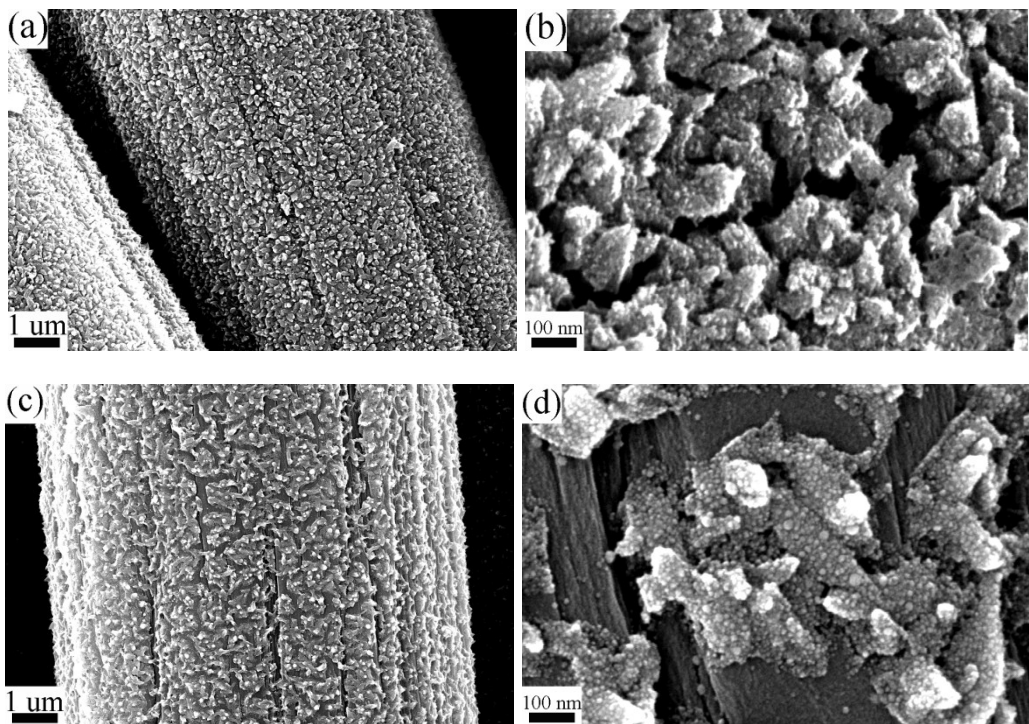


Figure S5. Morphological characterization. (a-b) FESEM images of FeCoNiCu MOFs/CC, (c-d) FESEM images of FeCoNiCu/CC.

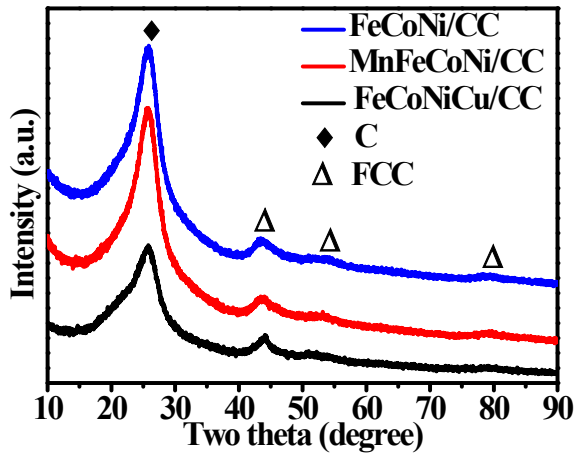


Figure S6. Phase structure characterization. XRD patterns of FeCoNi/CC, MnFeCoNi/CC and FeCoNiCu/CC.

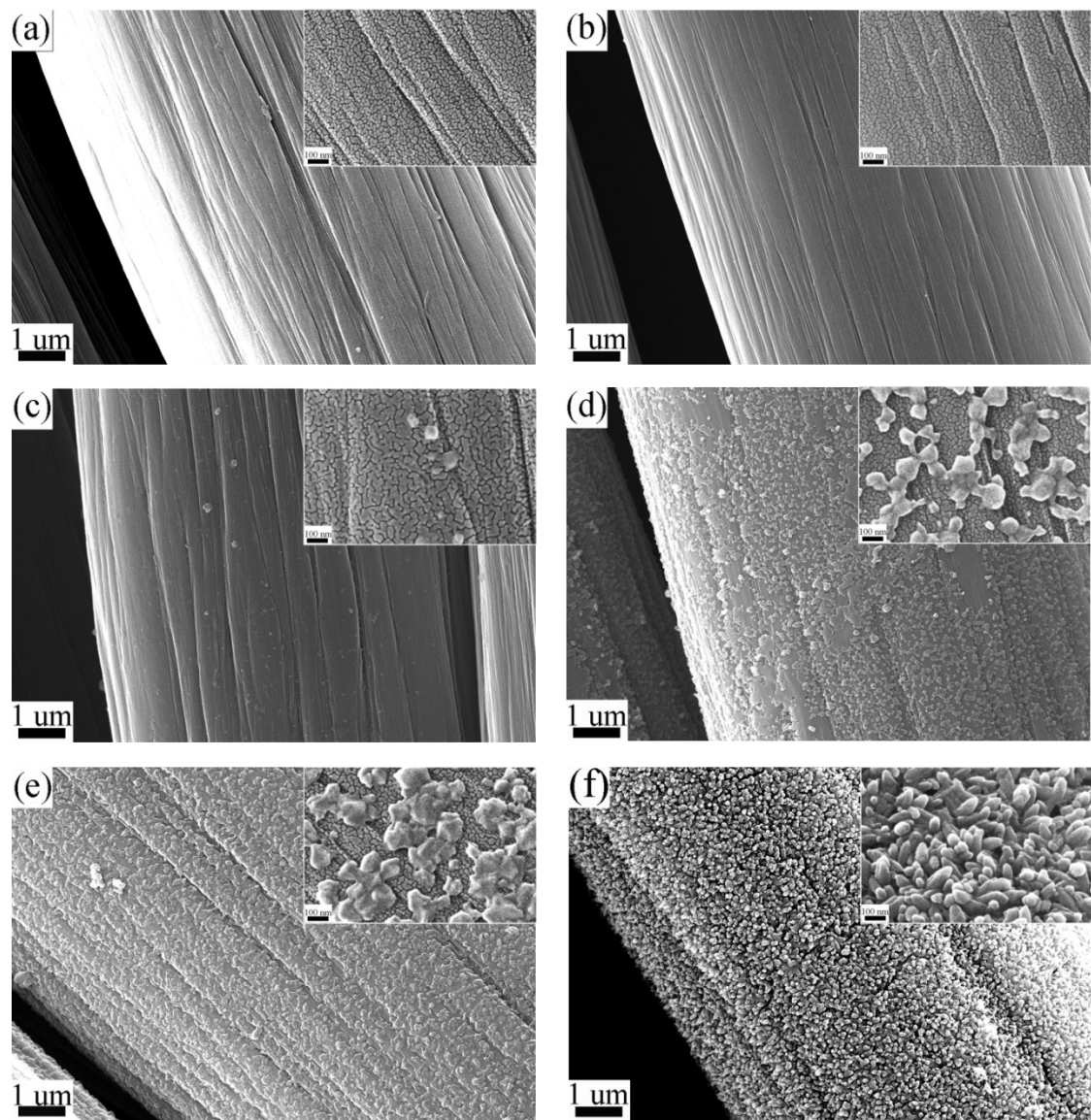


Figure S7. Morphological characterization. (a) FESEM images of bare carbon cloth, (b-f) FESEM images of quinary MOFs/CC at different solvothermal reaction. b 5 min, c 10 min, d 15 min, e 30 min, and f 60 min. Inset: corresponding high magnification FESEM images.

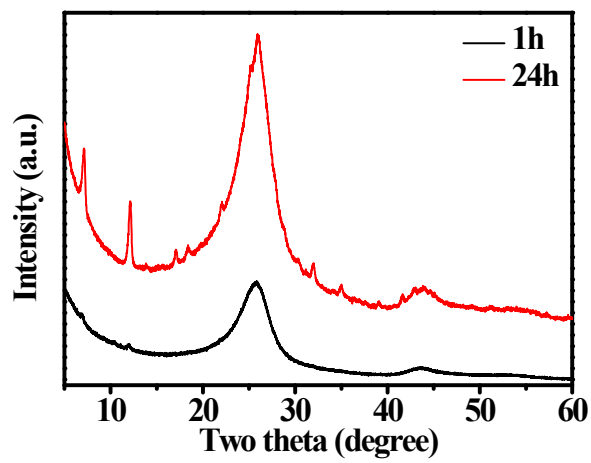


Figure S8. Phase structure characterization. XRD patterns of quinary MOFs/CC at different solvothermal reaction.

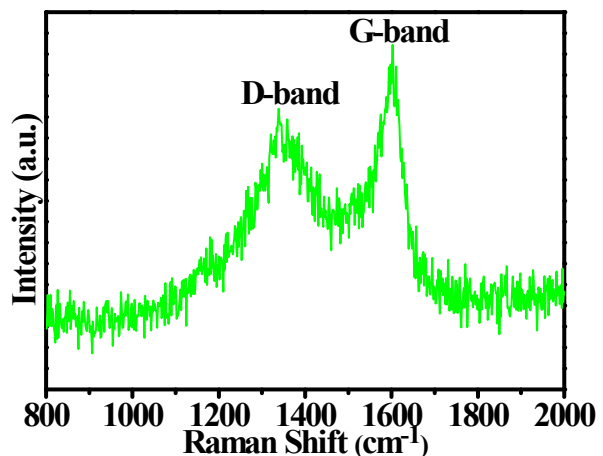


Figure S9. Carbon structure analysis of HEAN@NPC/CC-450 composites. Raman spectrum of HEAN@NPC/CC-450.

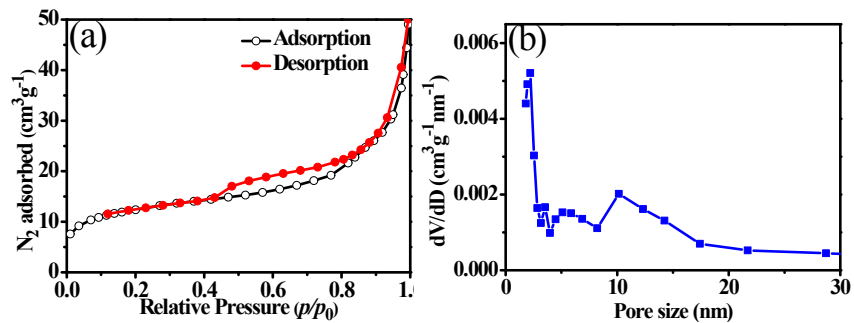


Figure S10. BET and porosity analysis of HEAN@NPC/CC-450 composites. (a) N_2 ad-/desorption isotherms, (b) Pore size distribution of HEAN@NPC/CC-450.

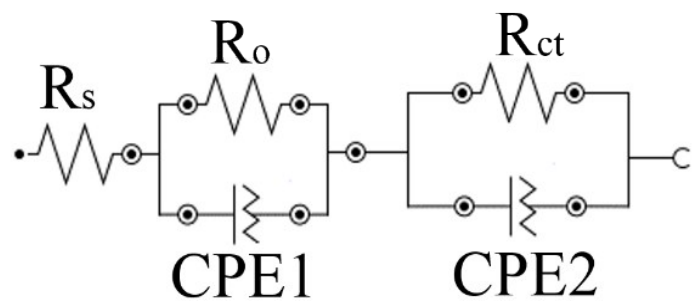


Figure S11. Equivalent electrical circuit of electrochemical impedance spectroscopy.

An equivalent electrical circuit used to model the OER process.

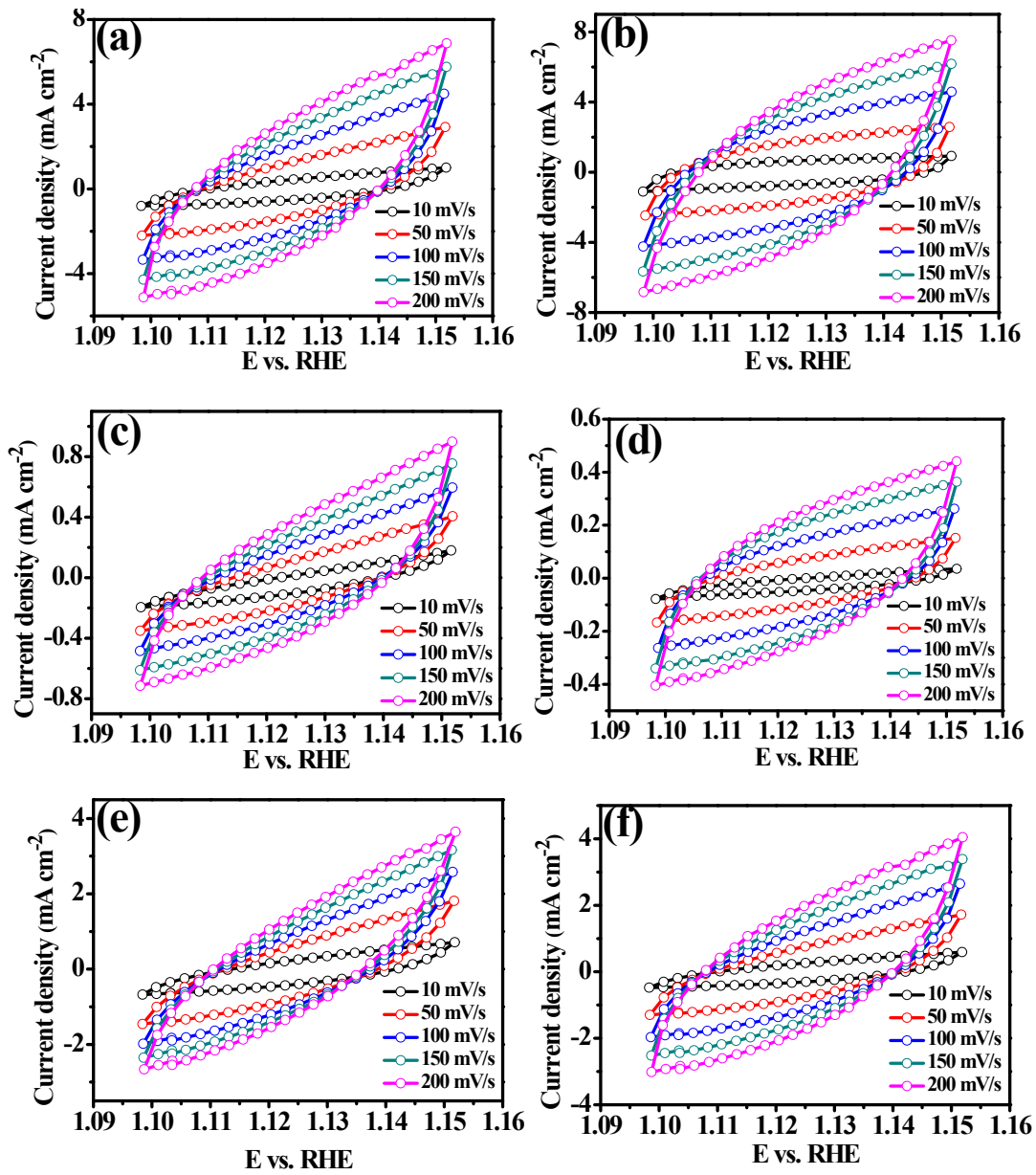


Figure S12. ECSA of electrocatalysts. (a-f) CV curves of the HEAN@NPC/CC-400, HEAN@NPC/CC-450, HEAN@NPC/CC-500, FeCoNi/CC, MnFeCoNi/CC, and FeCoNiCu/CC, respectively.

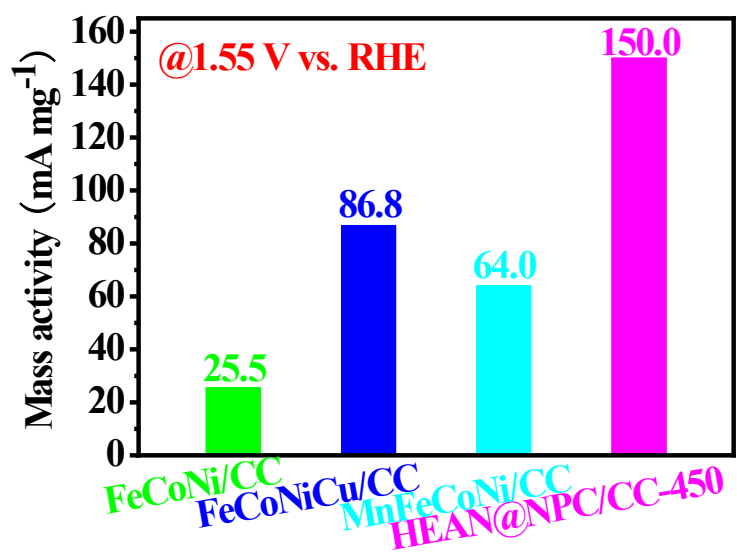


Figure S13. Mass activity. The mass activity of multimetal catalysts at 1.55 V vs. RHE.

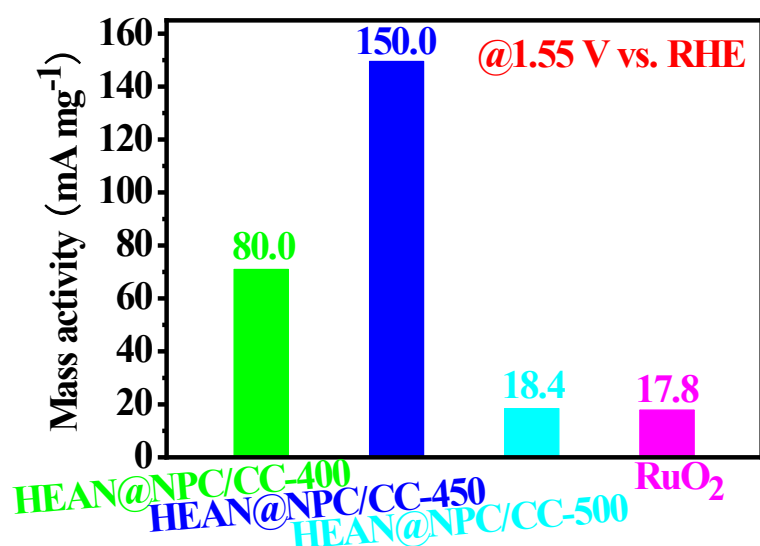


Figure S14. Mass activity. The mass activity of HEA catalysts at 1.55 V vs. RHE.

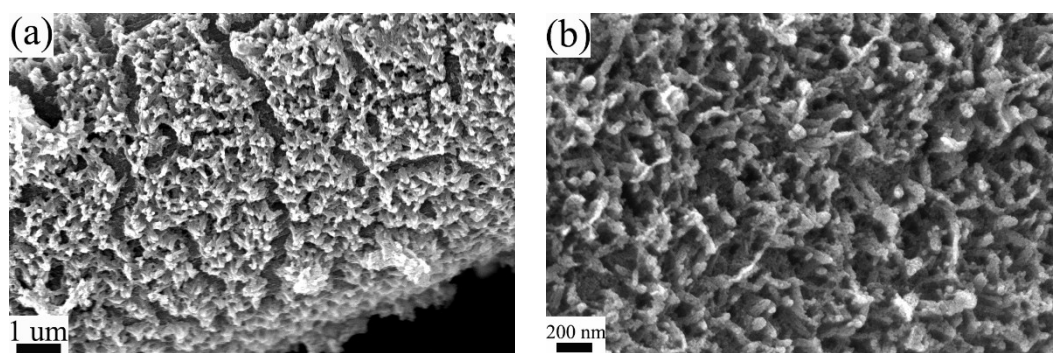


Figure S15. FESEM images of HEAN@NPC/CC-450 electrocatalyst after OER test.

Table S1. Overpotential, Tafel slope, charge transfer resistance, and double layer capacitance for electrocatalytic materials. The parameter of overpotential, Tafel slope, charge transfer resistance, and electrochemical double-layer capacitance for as-prepared electrocatalytic materials.

catalysts	η_{10} (mV)	Tafel slope (mV dec ⁻¹)	R_{ct} (Ω)	C_{dl} (mF cm ⁻²)
HEAN@NPC/CC-400	271	48	0.68	13.75
HEAN@NPC/CC-450	263	43	0.644	18.95
HEAN@NPC/CC-500	307	81	0.9	1.68
MnFeCoNi/CC	281	61	0.773	5.16
FeCoNiCu/CC	278	54	0.743	8.12
FeCoNi/CC	311	79	1.83	1.18
RuO ₂	277	59	4.01	

Table S2. Comparison of OER performance of HEAN@NPC/CC-450 catalyst with recently reported transition metal-based catalysts.

Materials	Electrolyte (KOH)	η_{10} (mV)	Tafel slope (mV dec ⁻¹)	Ref.
CoFeLaNiPt HEMG-NP	0.1 M KOH	377±4	150	S1
C@NCF-900	0.1 M KOH	430	66	S2
CoDNi-N/C	0.1 M KOH	360	72	S3
FeNi-NC	0.1 M KOH	380	115	S4
NiCo@N-C	0.1 M KOH	530	98	S5
CoFe-N-CN/CNTs	1 M KOH	285	51	S6
Fe-Ni@NC-CNTs	1 M KOH	274	45	S7
Ni _{0.9} Fe _{0.1} /NC	1 M KOH	330	45	S8
Mo _{0.6} Ni _{0.4}	1 M KOH	290	115	S9
NG-NiFe@MoC ₂	1 M KOH	320	31	S10
NiFe-MoO _x NS	1 M KOH	276	55	S11
FeCoNi	1 M KOH	288	60	S12
FeNi@NC	1 M NaOH	280	70	S13
NiFe@NDCHN	1 M KOH	270	64	S14
HEAN@NPC/CC-450	1 M KOH	263	43	This work

Details of Density functional theory computational

All energies are computed with the Vienna *Ab-initio* Simulation Package (VASP) suite of program (v5.4.4),^[S15, S16] Perdew–Burke–Ernzerhof (PBE)^[S17] exchange-correlation functional, and the projector augmented plane-wave method (PAW) with inactive core electrons described by hard pseudo-potentials constructed by Blöchl and Kresse.^[S18, S19] The PAW energy cutoff is set to 500 eV.

Since the Ni is the primary element of the HEAN, the perfect face centered cubic (FCC) of Ni is considered for the simulation to estimate the proximity of the free surface energy created by twin and dislocation defects. 2D periodic 11 layers of packing along the (1 1 1) direction, where Ni-Ni distances are 2.52 Å, are assumed. The Brillouin zone of the 2 periodic dimensions are sampled with a very dense K grid of about 0.016 Å⁻¹ via the Monkhorst–Pack scheme,^[S20] while the other dimension are separated by 20 Å of vacuum layer.

Table S3. 2-dimensional periodic Ni Density functional theory simulation summary

Defect	Perfect	Twin	Dislocation
Structure			
Lattice energy (eV/cell)	−58.0283	−58.0072	−57.9848
Free surface energy (J/m ²)	/	0.062	0.127

References

- [S1] M. W. Glasscott, A. D. Pendergast, S. Goines, A. R. Bishop, A. T. Hoang, C. Renault, J. E. Dick, *Nat. Commun.* **2019**, *10*, 2650.
- [S2] G. Nam, Y. Son, S. O. Park, W. C. Jeon, H. Jang, J. Park, S. Chae, Y. Yoo, J. Ryu, M. G. Kim, S. K. Kwak, J. Cho, *Adv. Mater.* **2018**, *30*, 1803372.
- [S3] Z. Li, H. He, H. Cao, S. Sun, W. Diao, D. Gao, P. Lu, S. Zhang, Z. Guo, M. Li, R. Liu, D. Ren, C. Liu, Y. Zhang, Z. Yang, J. Jiang, G. Zhang, *Appl. Catal. B Environ.* **2019**, *240*, 112.
- [S4] L. Yang, X. Zeng, D. Wang, D. Cao, *Energy Storage Mater.* **2018**, *12*, 277.
- [S5] Y. Fu, H. Y. Yu, C. Jiang, T. H. Zhang, R. Zhan, X. Li, J. F. Li, J. H. Tian, R. Yang, *Adv. Funct. Mater.* **2018**, *28*, 1705094.
- [S6] Y. Liu, F. Li, H. Yang, J. Li, P. Ma, Y. Zhu, J. Ma, *ChemSusChem* **2018**, *11*, 2358.
- [S7] X. Zhao, P. Pachfule, S. Li, J. R. J. Simke, J. Schmidt, A. Thomas, *Angew. Chem. Int. Ed.* **2018**, *57*, 8921.
- [S8] X. Zhang, H. Xu, X. Li, Y. Li, T. Yang, Y. Liang, *ACS Catal.* **2016**, *6*, 580.
- [S9] T. Zhang, X. Liu, X. Cui, M. Chen, S. Liu, B. Geng, *Adv. Mater. Interfaces* **2018**, *5*, 1800359.
- [S10] Q. Hu, X. Liu, B. Zhu, L. Fan, X. Chai, Q. Zhang, J. Liu, C. He, Z. Lin, *Nano Energy* **2018**, *50*, 212.
- [S11] C. Xie, Y. Wang, K. Hu, L. Tao, X. Huang, J. Huo, S. Wang, *J. Mater. Chem. A* **2017**, *5*, 87.

- [S12] Y. Yang, Z. Lin, S. Gao, J. Su, Z. Lun, G. Xia, J. Chen, R. Zhang, Q. Chen, *ACS Catal.* **2017**, *7*, 469.
- [S13] X. Cui, P. Ren, D. Deng, J. Deng, X. Bao, *Energy Environ. Sci.* **2016**, *9*, 123.
- [S14] L. Zhang, J. S. Hu, X. H. Huang, J. Song, S. Y. Lu, *Nano Energy* **2018**, *48*, 489.
- [S15] G. Kresse, J. Hafner, *Phys. Rev. B* **1993**, *48*, 13115.
- [S16] G. Kresse, J. Furthmüller, *Phys. Rev. B* **1996**, *54*, 11169.
- [S17] J. P. Perdew, K. Burke, M. Ernzerhof, *Phys. Rev. Lett.* **1996**, *77*, 3865.
- [S18] P. E. Blöchl, *Phys. Rev. B* **1994**, *50*, 17953.
- [S19] G. Kresse, J. Joubert, *Phys. Rev. B* **1999**, *59*, 1758.
- [S20] H. J. Monkhorst, J. D. Pack, *Phys. Rev. B* **1976**, *13*, 5811.